Progress In Electromagnetics Research, Vol. 113, 351–367, 2011

ELECTROMAGNETIC DESIGN AND ANALYSIS OF A NOVEL MAGNETIC-GEAR-INTEGRATED WIND POWER GENERATOR USING TIME-STEPPING FINITE ELEMENT METHOD

L. Jian and G. Xu

Shenzhen Institute of Advanced Integration Technology
Chinese Academy of Sciences
and The Chinese University of Hong Kong
1068 Xueyuan Avenue, University Town, Shenzhen, P. R. China

Y. Gong

Ningbo Tianan Electric Group Co., Ltd.
No. 1118 Tianan Road, Ningbo, Zhejiang, P. R. China

J. Song, J. Liang, and M. Chang

Shenzhen Institute of Advanced Integration Technology
Chinese Academy of Sciences
and The Chinese University of Hong Kong
1068 Xueyuan Avenue, University Town, Shenzhen, P. R. China

Abstract—This paper presents a novel permanent-magnet (PM) machine for wind power generation. In order to achieve high power/torque density as well as get rid of the nuisances aroused by the mechanical gearbox, a coaxial magnetic gear (CMG) is engaged. Different from the existing integrated machine in which armature windings are deployed in the inner bore of the CMG as an individual part, stator windings are directly inserted among the slots between the ferromagnetic segments in this proposed machine. Thus, it can offer several merits, such as simpler mechanical structure, better utilization of PM materials and lower manufacturing cost. Moreover, by artfully designing the connection of the armature windings, the electromagnetic coupling between the windings and the outer rotor PMs can be dramatically decreased, and the electromechanical energy conversion can be achieved by the field interaction between the inner rotor PMs and the armature windings.

Received 16 December 2010, Accepted 1 February 2011, Scheduled 8 February 2011
Corresponding author: Linni Jian (ln.jian@siat.ac.cn).

1. INTRODUCTION

With the great concern on global warming and energy crisis, wind power generation has attracted increasing attention [1]. Generally, wind power generation can be classified as constant-speed constant-frequency (CSCF) wind power generation and variable-speed constant-frequency (VSCF) wind power generation. In the CSCF system, squirrel-cage induction generator is usually adopted [2]. It benefits from its simple structure and high robustness. However, since the turbine speed is kept constant regardless of the variation of the wind speed, the CSCF system suffers from very low efficiency and high mechanical stress. On the contrary, the efficiency of the VSCF system is much higher, since the turbine speed changes with the wind speed to capture the maximum wind power. For the VSCF system, several types of generators have been adopted or proposed, such as the doubly fed induction machine [3], switched reluctance machine [4], doubly salient PM machine [5], PM hybrid machine [6] and double-stator PM machine [7]. However, mechanical gears are generally engaged to match the low-speed operation of the wind turbine and the relatively high-speed operation of the generator. This not only increases the cost of manufacture and maintenance, but also reduces the efficiency and robustness. Although low-speed directly driven PM machine has been proposed to get rid of the nuisances aroused by mechanical gear [8], it still suffers from heavy weight, bulky size and high manufacturing cost.

Recently, the concept of coaxial magnetic gears (CMG) has been proposed [9–12]. It can achieve non-contact transmission by the interaction of magnetic fields. Thus, it offers some distinct advantages: namely, minimum acoustic noise, free from maintenance, improved reliability, and inherent overload protection. Very recently, it has been applied in electric vehicles, such as the integrated in-wheel motor [13] and the electric-continuously variable transmission system [14]. In [15], CMG has been integrated into a PM motor to offer high-torque low-speed operation and wind power generation.

The purpose of this paper is to propose a novel magnetic-gear-integrated wind power generator (MGIG). The armature windings are directly inserted in the air-slots on the modulating ring of the CMG. Moreover, the windings are designed to possess the same pole-pair number with the inner rotor PM. Thus, by the field interaction between the inner rotor PMs and the armature windings, the electromechanical energy conversion can be achieved. Compared with the integrated machine presented in [15], the proposed generator is with simpler mechanical structure, better utilization of PM materials and lower

manufacturing cost. In Section 2, several typical PM wind power generators will be introduced and discussed. After that, the design details and the operating principle of the proposed will be elaborated in Section 3. Section 4 will be devoted to analyze the electromagnetic characteristics by using time-stepping finite element method (TS-FEM) [16–20]. In Section 5, comparisons between the proposed generator and its existing counterparts are made. Finally, conclusion will be drawn in Section 6.

2. PM WIND POWER GENERATORS

Compared with induction generators [21] and switched reluctance machines, permanent magnet [22] wind power generators benefit from their high efficiency and high power density. In practical applications, the weight, volume and cost of the generation system are great concerns. For a certain power rating, the higher rotor rotational speed implies lower electromagnetic torque. According to the electric machine design principles, the electromagnetic torque is proportional to the volume of the machine. Hence, improving the rated rotor speed could reduce the machine volume, thus, the weight and manufacture cost. For this reason, as shown in Fig. 1(a), mechanical gearbox is usually engaged to scale up the low-speed of the wind turbine, so as that, the generator can be designed to be a high-speed (about 2000 rpm) machine, which can offer very high power density. Herein, a 6-pole 27-slot PM generator is shown for example. However, as aforementioned, mechanical gearbox can be very troublesome. Therefore, directly-driven PM wind power generator (DDPMG) is attracting increasing attention. As shown in Fig. 1(b), a 20-pole 48-slot out-rotor DDPMG is given for example. Due to the absence of gearbox, the rated speed of DDPMG is rather slow (less than 200 rpm). Thus, it is with much heavier weight and much bigger volume.

CMG is an emerging device. It can achieve speed variation, just like mechanical gearbox. Moreover, it can overcome the nuisances aroused by mechanical gearboxes due to the non-contact torque transmission resulted from the interaction of magnetic fields. Therefore, it is quite natural for people to investigate the potential application of CMG in wind power generation. Fig. 2 shows the magnetic-geared integrated generation proposed in [15]. Differing from simply connecting the CMG to a high-speed generator, the stator of the generator is directly inserted into the inner bore of the CMG. Moreover, the CMG shares its inner rotor with the generator. This compact design can offer very high power density. Nevertheless, its mechanical structure is too complicated: it consists of four concentric

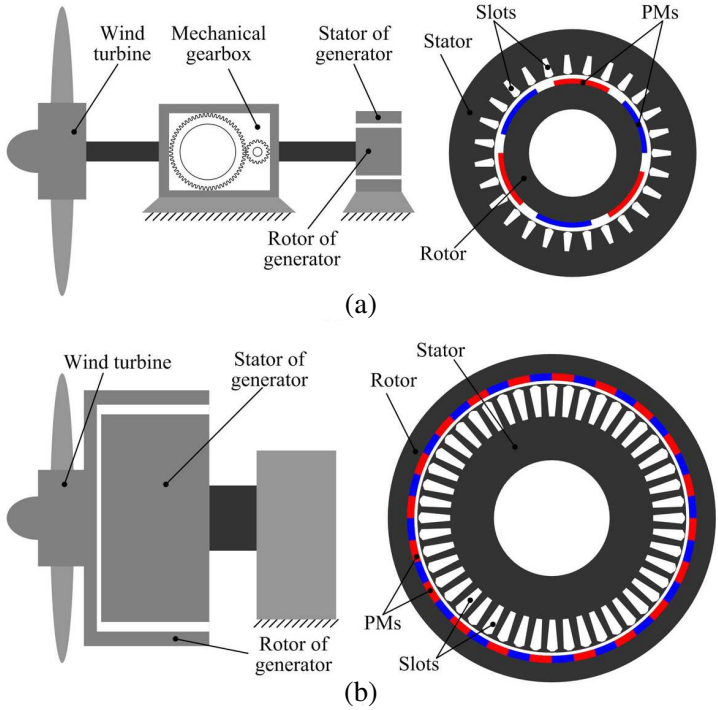

Figure 1. Traditional PM wind power generation system. (a) Mechanical-gear-driven generator. (b) Directly-driven generator.

parts, including the outer rotor, the modulating ring, the inner rotor and the stator. What is more, it consumes too many permanent magnets.

In what follows, a new magnetic-gear-integrated generator will be presented. Its topology and working principle will be elaborated.

3. SYSTEM DESIGN AND OPERATING PRINCIPLE

3.1. System Design

Figure 3 shows the configuration of the proposed wind power generation system. It consists of the wind turbine, the proposed magnetic-gear-integrated generator (MGIG) and the electrical cabinet. While the electrical cabinet includes a three-phase bridge rectifier to perform AC-DC conversion, a DC-DC converter to regulate the rectified DC voltage, a battery pack for energy storage, and an inverter to perform DC-AC conversion.

Figure 4 illustrates the cross section view of the proposed MGIG. It contains four main parts: the outer rotor, the inner rotor, the stator, and the armature windings. PMs are mounted on the inside surface and the outside surface of the outer rotor and inner rotor, respectively. The stator is composed of several ferromagnetic segments which are symmetrically deployed in the space between the inner rotor and the outer rotor. The inner and outer metal casings and the left and the right end plates are employed so as to form a whole stator. For compact

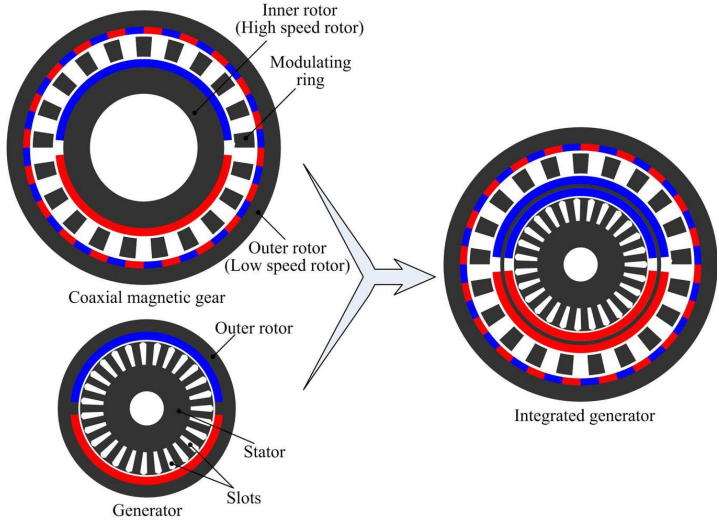

Figure 2. Magnetic-geared Integrated PM generator.

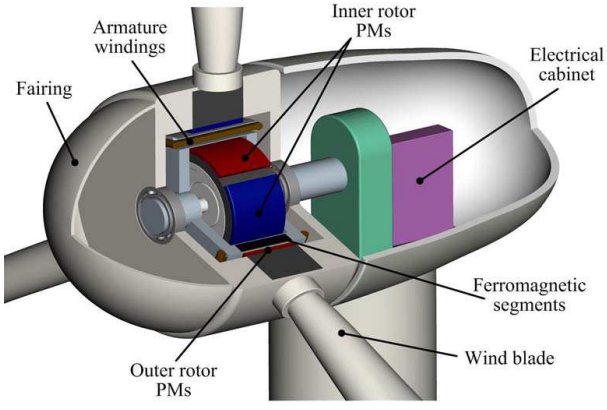

Figure 3. Proposed wind power generation system.

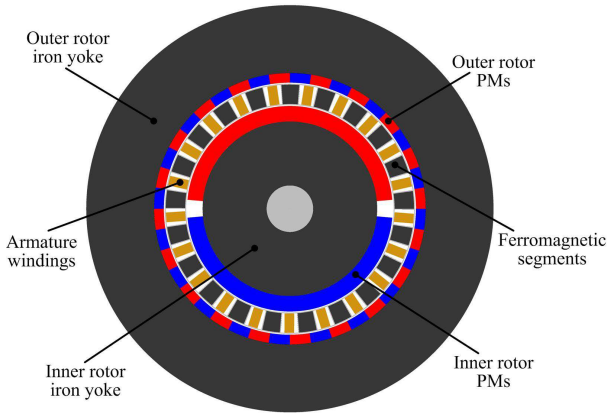

Figure 4. Cross section view of proposed MGIG.

design, the wind blades are directly mounted on the outer rotor of the MGIG, while the fairing is equipped on the front end of the stator. The armature windings are inserted into the air slots between the ferromagnetic segments.

3.2. Operating Principle

By defining p_1, p_2 as the pole-pair numbers of the outer rotor PMs and inner rotor PMs, respectively, and n_s as the number of ferromagnetic segments on the stator, as long as they satisfy:

$$n_s = p_1 + p_2 \tag{1}$$

The so-called magnetic gearing effect will occur, and the corresponding speed relationship can be expressed as:

$$\omega_2 = -G_r \omega_1 \tag{2}$$

$$G_r = \frac{p_1}{p_2} \tag{3}$$

where ω_1, ω_2 are the rotational speeds of the outer rotor and inner rotor respectively, and G_r is the gear ratio. The minus sign indicates that the two rotors rotate in opposite directions.

In the proposed MGIG, the pole-pair number p_1, p_2 and the number of ferromagnetic segments n_s are chosen as 20, 1 and 21 respectively. Thus, the gear ratio of 20:1 is resulted. Table 1 gives the specification of the proposed MGIG, it can be seen that the rated speed of the wind turbine is 150 rpm, while the rated speed of the inner rotor is 3000 rpm. Fig. 5 illustrates the stator winding connection in the stator. The three-phase symmetric windings consist of 21 double-layer

Table 1. Specifications of proposed MGIM.

Rated speed of inner rotor	3000 rpm
Rated speed of outer rotor	150 rpm
Rated power	10 kW
Rated phase voltage	380 V
Rated frequency	50 Hz
Axial length	140 mm
Diameter of house	420 mm
Remanence of PMs	1.1 T

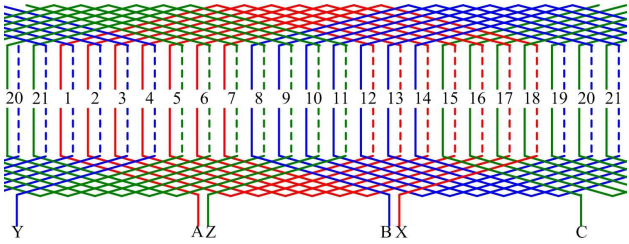

Figure 5. Armature winding connection.

coils. The pole-pair number of the windings is designed to be 1, which is equal to that of the PMs on the inner rotor. Thus, by the interaction of the electromagnetic fields excited by the inner rotor PMs and the armature windings, stable electromechanical energy conversion can be achieved. Because of the different pole-pair numbers of the windings and the outer rotor PMs, the rotation of the outer rotor will have little impact on the electric power generation. This will be elaborated in the Section 3 by using FEM.

From Fig. 3 and Fig. 1(b), it can be found that the key difference between the proposed MGIG and the DDPMG lies in that the MGIG has a high-speed inner rotor but the DDPMG did not. From the angle of power flow, the wind power is transmitted from outer rotor to inner rotor, and then, the electromechanical energy conversion is achieved by the interaction between the inner rotor and the armature windings. In this sense, the inner rotor serves as the bridge of the energy conversion.

4. TIME-STEPPING FINITE ELEMENT ANALYSIS

Finite element method [23–25] is a mature numerical tool for solving electromagnetic field problems. It has been extensively employed for

designing and analyzing electromagnetic devices, such as antenna [26], waveguide filter [27] and so forth. In this section, TS-FEM is engaged for analyzing the electromagnetic characteristics of the proposed MGIG. The calculation model consists of two equations: the finite element equation of the electromagnetic field of the proposed MGIG, and the circuit equation of the armature windings. The two-dimensional electromagnetic equation is governed by:

Ω:

$$\frac{\partial}{\partial x}(\gamma\frac{\partial A}{\partial x})+\frac{\partial}{\partial y}(\gamma\frac{\partial A}{\partial y})=-J-\gamma(\frac{\partial B_{ry}}{\partial x}-\frac{\partial B_{rx}}{\partial y})+\sigma\frac{\partial A}{\partial t} \tag{4}$$

s:

$$A=0 \tag{5}$$

where Ω is the region of calculation, A the magnetic vector potential component along the z axis, J the current density, γ the reluctivity, the electrical conductivity, B_{rx} and B_{ry} the remnant flux density components of the PM along the x axis and y axis, and s the boundary of the region of calculation.

Then, the back-electromotive force (Back-EMF) of the armature winding can be calculated by:

$$e=-\frac{L}{S}\left(\iint_{\Omega+}\frac{\partial A}{\partial t}d\Omega-\iint_{\Omega-}\frac{\partial A}{\partial t}d\Omega\right) \tag{6}$$

where e is the Back-EMF produced by one coil, L is the axial length of the machine, S is the area of the stator conductor, $\Omega+$ and $\Omega-$ are the cross sectional areas of 'go' and 'return' conductor of the coil.

When taking into account the electric loads, the stator phase circuit equation can be given by:

$$V_s=Ne-R_\sigma i_s-L_\sigma\frac{di_s}{dt}=R_l i_s+L_l\frac{di_s}{dt} \tag{7}$$

where N is the number of the coils, V_s is the phase voltage, i_s is the phase current, R_σ, L_σ are the resistance and the inductance of the phase winding, respectively, R_l and L_l are the resistance and the inductance of the electric load.

Figure 6 shows the magnetic field distributions of the proposed MGIG, in which, Fig. 6(a) gives the Case 1: open-circuit and all PMs are magnetized, Fig. 6(b) gives the Case 2: open-circuit and only PMs on inner rotor are magnetized, Fig. 6(c) gives the Case 3: open-circuit and only PMs on outer rotor are magnetized, Fig. 6(d) gives the Case 4: full-loaded and all PMs are magnetized. It can be observed from Fig. 6(c) that due to the modulation effect aroused by the ferromagnetic segments, the magnetic field excited by the PMs on the outer rotor contains a space harmonic component with pole-pair

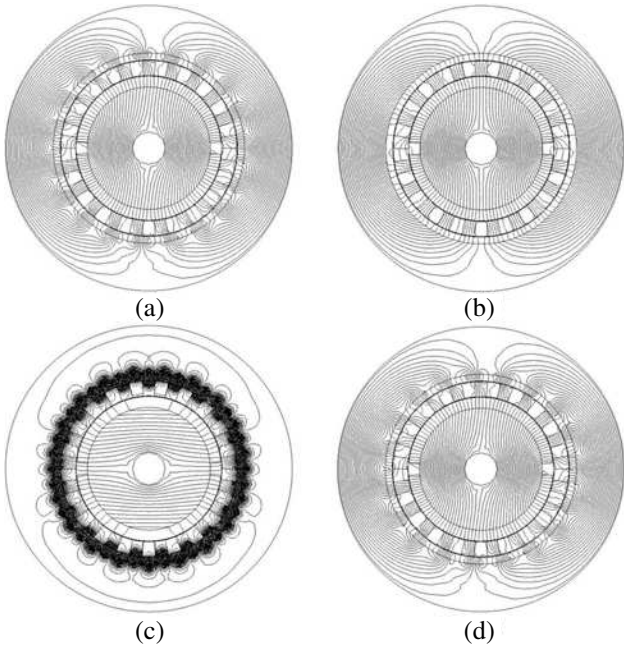

Figure 6. Magnetic field distribution. (a) Case 1. (b) Case 2. (c) Case 3. (d) Case 4.

number equal to 1. This harmonic component will interact with the magnetic field excited by the PMs on the inner rotor, as so to achieve stable torque transmission as well as speed variation.

Figure 7 illustrates the radial flux density waveforms in the inner airgaps and the outer airgaps in Case 1, 2 and 3. By calculating the Maxwell's stress tensors in the two airgaps, the torque transmission capability between the inner rotor and the outer rotor can be determined. While keeping the outer rotor standstill, the inner rotor is rotated step by step. The corresponding torque-angle curves are calculated as shown in Fig. 8(a). It can be found that the torque-angle curves vary sinusoidally, in which the maximum torque values denote the pull-out torques. On the inner rotor and the outer rotor, the pull-out torques are 58.65 Nm and 1156.17 Nm, respectively. Their ratio is 1:19.7, which has a good agreement with the ratio of pole-pair numbers of two rotors equal to 1:20. Fig. 8(b)gives the torque versus time waveforms when the outer rotor and the inner rotor are rotating at 3000 rpm and −150 rpm, respectively. It can be found that the torque ripple on the inner rotor is more obvious than that on the outer rotor.

In order to verify the validity of the proposed MGIG, the coupling

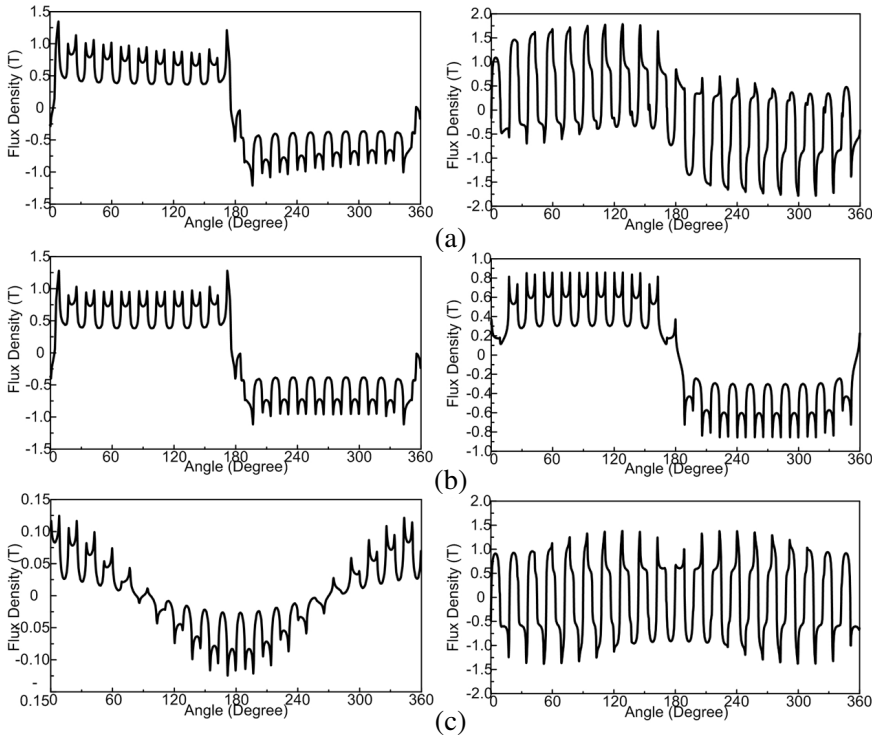

Figure 7. Flux density waveforms in airgaps: Left shows the waveforms in inner airgap, right shows the waveforms in outer airgap. (a) Case 1. (b) Case 2. (c) Case 3.

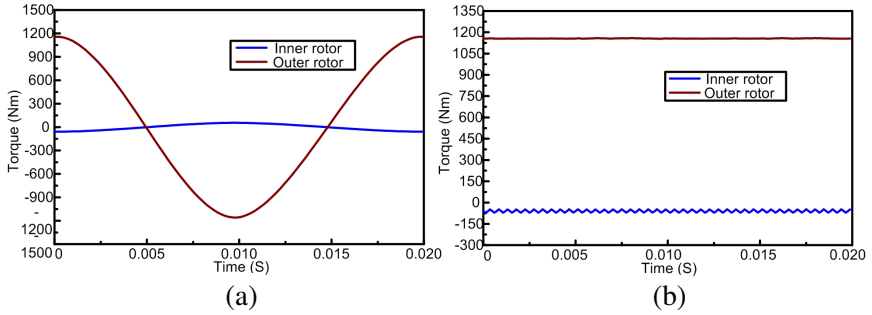

Figure 8. Torque transmission capability. (a) Torque-angle curves. (b) Stable torque waveforms.

of the armature windings and the PMs on the two rotors have been investigated. Fig. 9(a) shows the back-EMF waveforms for Case 1, 2, and 3, when the two rotors rotating at 150 rpm and 3000 rpm,

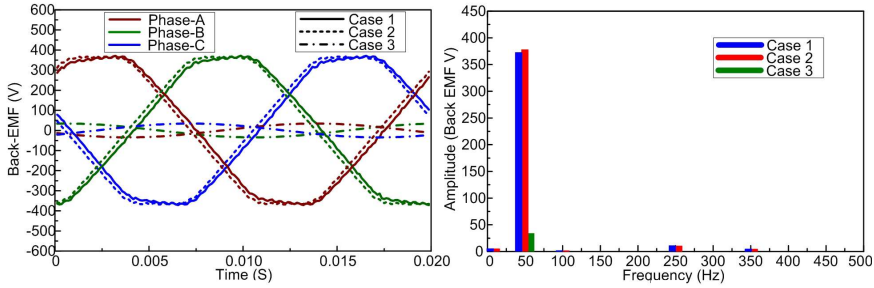

Figure 9. Back-EMF. (a) Waveforms. (b) Harmonic spectra.

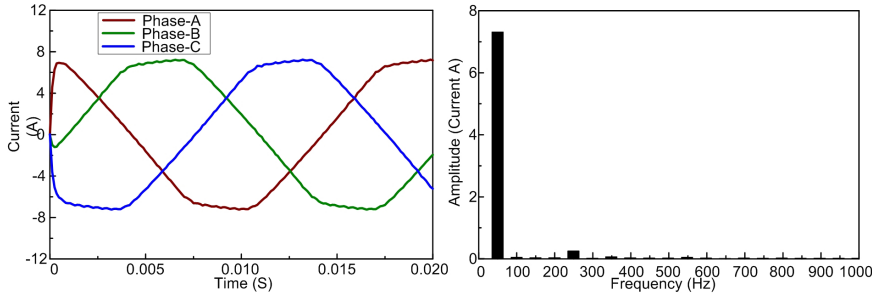

Figure 10. Phase current. (a) Waveforms. (b) Harmonic spectrum.

respectively. Their harmonic spectra are obtained by using fast Fourier transform (FFT) as given in Fig. 9(b). It can be found that there is no significant difference between the back-EMF waveforms deduced by the PMs on the two rotors together or only by the PMs on the inner rotor. The amplitudes of the fundamental component (Frequency=50 Hz) of the back-EMF waveforms in Case 1, 2 and 3 equal 375.2 V, 382.7 V and 34.2 V, respectively. This demonstrates that by artfully designing the connection of the armature windings, the impact of the rotation of the outer rotor on the electrical power generation can be dramatically decreased. The phase current waveforms are illustrated in Fig. 10(a). In this case, the resistive load of 50 Ω per phase is connected to the machine. Fig. 10(b) shows the harmonic spectrum.

The losses occurred in the proposed machine has also been investigated. Assuming the generator working at rated speeds ($\omega_1 = 150$ rpm, $\omega_2 = -3000$ rpm,) and with load current $I = 20$ A, Fig. 11(a) shows the calculated iron losses density distribution (including the eddy current loss and magnetic hysteresis loss) in the iron yokes of both rotors and the ferromagnetic segments of the modulating ring.

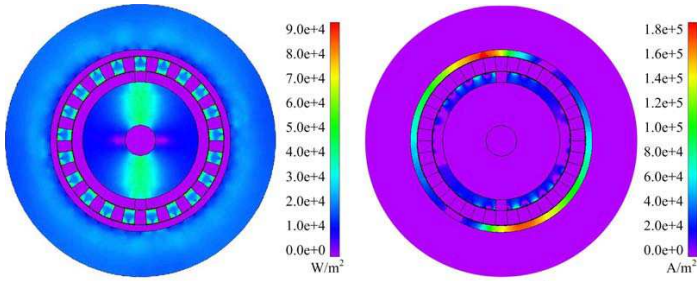

Figure 11. Losses at full load. (a) Iron losses density in iron yokes. (b) Eddy current density in PMs.

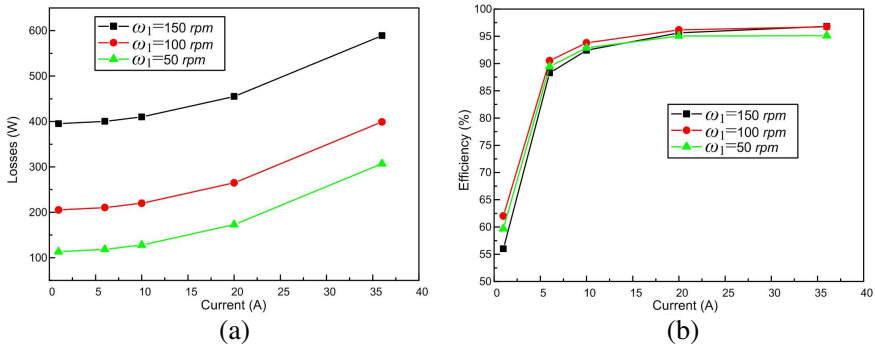

Figure 12. (a) Losses at different working points. (b) Efficiency at different working points.

Fig. 11(b) gives the calculated eddy current density distribution in the PMs. Fig. 12(a) illustrates the losses (including iron losses in iron yokes and eddy current losses in PMs) under different working points. When ignoring the mechanical losses, the corresponding efficiency can be deduced as shown in Fig. 12(b).

5. COMPARISONS

The existing MGIG and the DDPMG shown in Fig. 2 and Fig. 1(b) are modeled by using FEM for comparing with the proposed MGIG. For fair comparison, the radius of the outer airgap and the housing, the thickness and pole-pairs of the PMs on the outer rotor, and the number of conductors of the armature windings of these three models are the same. Moreover, for the two MGIGs, the size and shape of the modulating rings and the pole-pairs of the PMs on the inner rotor are

also the same.

Figure 13 shows the magnetic field distributions at no-load. It indicates that the iron yoke of the outer rotor of the DDPMG is not fully utilized, which means the size of the housing of the DDPMG could be reduced a little bit. Nevertheless, this can also be achieved for the MGIGs when other combination of pole-pair numbers of the PMs is adopted. This will be further investigated in our follow-up work. When rotating at 150 rpm (Outer rotor), the calculated back-EMF waveforms are shown in Fig. 14. Since the MGIGs combine the magnetic-gear effect, the rotational speeds have been scaled up dramatically, and the magnitudes of the back-EMF of the MGIGs are much higher than that of the DDPMG. By injecting three-phase ac current $I = 20$ A into the armature windings of these three machines, and keeping the rotational speeds equal to 150 rpm (Outer rotor), the calculated maximum output electromagnetic torques are illustrated in Fig. 15. It can be observed that the average values of the output torques are 65 Nm, 400 Nm and 684 Nm, respectively. This indicates that the proposed MGIG can offer

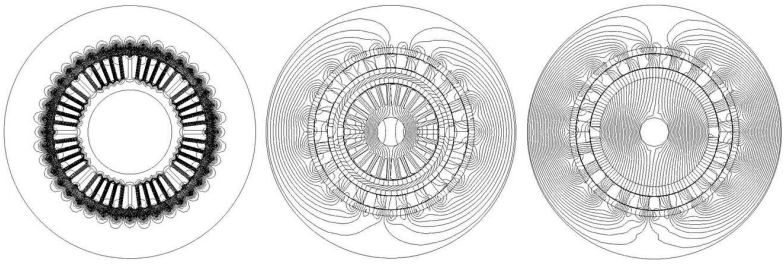

Figure 13. Magnetic field distributions at no-load. (a) DDPMG. (b) Existing MGIG. (c) Proposed MGIG.

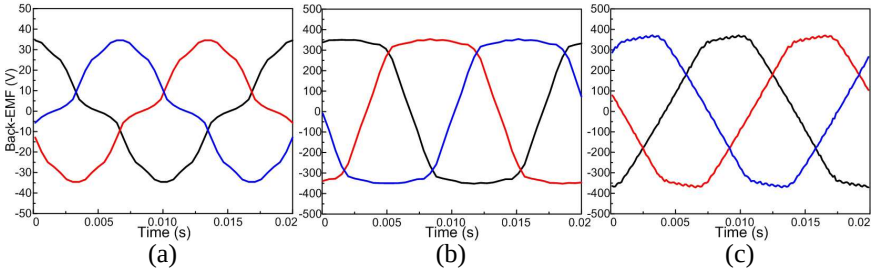

Figure 14. Back-EMF waveforms. (a) DDPMG. (b) Existing MGIG. (c) Proposed MGIG.

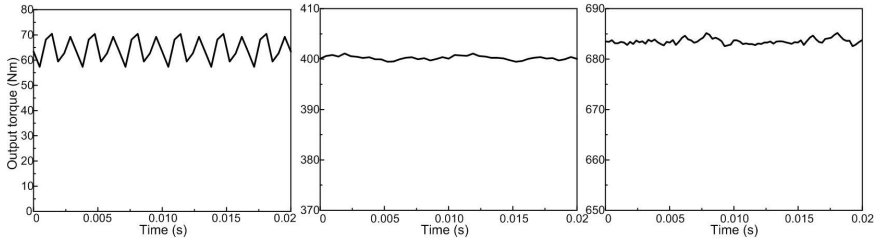

Figure 15. Electromagnetic torque waveforms. (a) DDPMG. (b) Existing MGIG. (c) Proposed MGIG.

the biggest torque/power density.

Finally, the losses occurred in the DDPMG and the existing MGIG at full-load have been calculated. Compared with the loss equal to 458 W for the proposed MGIG as shown in Fig. 12(a), the losses for the DDPMG and the existing MGIG are equal to 382 W and 496 W, respectively.

6. CONCLUSIONS

In this paper, a novel permanent-magnet (PM) machine for wind power generation has been proposed and analyzed. Compared with the traditional wind power generators, it can offer following advantages:

1) The low-speed outer-rotor topology can enable direct coupling with the wind blades to capture wind power with high efficiency.
2) The integrated coaxial magnetic gear can scale up the rotational speed with very big gear ratio, thus to achieve ultra-high power density of the whole system.
3) The non-contact torque transmission of the integrated coaxial magnetic gear can offer merits of minimum acoustic noise, free from maintenance, improved reliability, and inherent overload protection.
4) The armature windings are directly inserted into the air-slots among the ferromagnetic segments, as so to achieve simpler mechanical structure, better utilization of PM materials and lower manufacturing cost.

The design details and operating principle of the proposed machine are elaborated. By using the time-stepping finite element method (TS-FEM), the electromagnetic characteristics are analyzed. The results verify the validity of the proposed machine.

ACKNOWLEDGMENT

The first author of this paper would like to thank Prof. K. T. Chau and Prof. C. C. Chan at The University of Hong Kong for their precious guidance, assistance and encourage over the past years.

REFERENCES

1. Negra, N., O. Holmstrom, B. Birgitte, and S. Poul, "Windfarm generation assessment for reliability analysis of power systems," *Wind Engineering*, Vol. 31, No. 6, 383–400, 2007.
2. Grauers, A., "Efficiency of three wind energy generator systems," *IEEE Trans. Energy Conversion*, Vol. 11, No. 3, 650–657, 1996.
3. Muller, S., "Doubly fed induction generator system for wind turbines," *IEEE Ind. Appl. Magazine*, Vol. 8, No. 3, 26–33, 2002.
4. Torrey, D., "Switched reluctance generators and their control," *IEEE Trans. Ind. Electron.*, Vol. 49, No. 1, 3–13, 2002.
5. Fan, Y., K. T. Chau, and M. Cheng, "A new three-phase doubly salient permanent magnet machine for wind power generation," *IEEE Trans. Ind. Appl. Magazine*, Vol. 42, No. 1, 53–59, 2006.
6. Chau, K. T., Y. Li, J. Jiang, and S. Niu, "Design and control of a PM brushless hybrid generator for wind power application," *IEEE Trans. Magn.*, Vol. 42, No. 10, 3497–3499, 2006.
7. Niu, S., K. T. Chau, J. Jiang, and C. Liu, "Design and control of a new double-stator cup-rotor permanent-magnet machine for wind power generation," *IEEE Trans. Magn.*, Vol. 43, No. 6, 2501–2503, 2007.
8. Chen, J., C. V. Nayar, and L. Xu, "Design and finite-element analysis of an outer-rotor permanent magnet generator for directly coupled wind turbines," *IEEE Trans. Magn.*, Vol. 36, No. 5, 3802–3809, 2000.
9. Atallah, K., S. Calverley, and D. Howe, "Design, analysis and realization of a high-performance magnetic gear," *IEE Proc. Electric Power Appl.*, Vol. 151, No. 2, 135–143, 2004.
10. Jian, L. and K.-T. Chau, "Analytical calculation of magnetic field distribution in coaxial magnetic gears," *Progress In Eletromagnetics Research*, Vol. 92, 1–16, 2009.
11. Jian, L. and K. T. Chau, "A coaxial magnetic gear with halbach permanent-magnet arrays," *IEEE Trans. Energy Conversion*, Vol. 25, No. 2, 319–328, 2010.
12. Jian, L., K. T. Chau, W. Li, and J. Li, "A novel coaxial magnetic

gear using bulk HTS for industrial applications," *IEEE Trans. Appl. Superconduc.*, Vol. 20, No. 3, 981–984, 2010.

13. Chau, K. T, D. Zhang, J. Jiang, C. Liu, and Y. Zhang, "Design of a magnetic-geared outer-rotor permanent-magnetic brushless motor for electric vehicles," *IEEE Trans. Magn.*, Vol. 43, No. 6, 2504–2506, 2007.
14. Jian, L. and K.-T. Chau, "Design and analysis of a magnetic-geared electronic-continuously variable transmission system using finite element method," *Progress In Eletromagnetics Research*, Vol. 107, 47–61, 2010.
15. Jian, L., K. T. Chau, and J. Jiang, "A magnetic-geared outer-rotor permanent-magnet brushless machine for wind power generation," *IEEE Trans. Ind. Appl.*, Vol. 45, No. 3, 954–962, 2009.
16. Faiz, J. and B. M. Ebrahimi, "Mixed fault diagnosis in three-phase squirrel-cage induction motor using analysis of air-gap magnetic field," *Progress In Eletromagnetics Research*, Vol. 64, 239–255, 2006.
17. Vaseghi, B, N. Takorabet, and F. Meibody-Tabar, "Transient finite element analysis of induction machines with stator winding turn fault," *Progress In Eletromagnetics Research*, Vol. 95, 1–18, 2009.
18. Faiz, J., B. M. Ebrahimi, and M. B. B. Sharifian, "Time stepping finite element analysis of broken bars fault in a three-phase squirrel-cage induction motor," *Progress In Eletromagnetics Research*, Vol, 68, 53–70, 2007.
19. Chari, M. V. K., G. Bedrosian, J. D'Angelo, A. Konrad, G. M. Cotzas, and M. R. Shah, "Electromagnetic field analysis for electrical machine design," *Progress In Eletromagnetics Research*, Vol. 04, 159–211, 1991.
20. Touati, S., R. Ibtiouen, O. Touhami, and A. Djerdir, "Experimental investigation and optimization of permanent magnet motor based on coupling boundary element method with permeances network," *Progress In Eletromagnetics Research*, Vol. 111, 71–90, 2011.
21. Lecointe, J.-P., B. Cassoret, and J. F. Brudny, "Distinction of toothing and saturation effects on magnetic noise of induction motors," *Progress In Eletromagnetics Research*, Vol. 112, 125–137, 2011.
22. Ravaud, R. and G. Lemarquand, "Comparsion of the coulombian and amperian current models for calculating the magnetic field produced by radially magnetized arc-shaped permanent magnets," *Progress In Eletromagnetics Research*, Vol. 95, 309–327, 2009.

23. Tian, J., Z.-Q. Lv, X.-W. Shi, L. Xu, and F. Wei, "An efficient approach for multiforntal algorithm to solve non-positive-definite finite element equations in electromagnetic problems," *Progress In Eletromagnetics Research*, Vol. 95, 121–133, 2009.
24. Ping, X. W. and T.-J. Cui, "The factorized sparse approximate inverse preconditioned conjugate gradient algorithm for finite element analysis of scatering problems," *Progress In Eletromagnetics Research*, Vol. 98, 15–31, 2009.
25. Chen, J. and Q. H. Liu, "A non-spurious vector spectral element method for maxwell's equations," *Progress In Eletromagnetics Research*, Vol. 96, 205–215, 2009.
26. Chau, Y.-F., H.-H. Yeh, and D. P. Tsai, "A new type of optical antenna: plasmonics nanoshell bowtie antenna with dielectric hole," *Journal of Electromagnetic Waves and Applications*, Vol. 24, No. 11–12, 1621–1632, 2010.
27. Khalilpour, J. and M. Hakkak, "Controllable waveguide bandstop filter using S-shaped ring resonators," *Journal of Electromagnetic Waves and Applications*, Vol. 24, No. 5–6, 587–596, 2010.